Off-field Testing of Grid Scenarios at Medium Voltage in Flexible AC Transmission Systems involving Wind Energy

[1,2]Lorenzen, Helge; [3]Timmerberg, Josef; [4]Lüken, Tim; [5]Mylvaganam, Saba

[1]Department of Engineering Sciences - Jade University of Applied Sciences
[2]Department of Electrical engineering, Information Technology and Cybernetics - University of South-Eastern Norway
[3]Department Management, Information, Technology - Jade University of Applied Sciences
[4]Strategic Net Development - EWE NETZ GmbH
[5]Department of Electrical engineering, Information Technology and Cybernetics - University of South-Eastern Norway

Lorenzen, H., Timmerberg, J., Lüken, T., & Mylvaganam, S. (2019). *Off-field Testing of Grid Scenarios at Medium Voltage in Flexible AC Transmission Systems involving Wind Energy*. 2019 International IEEE Conference and Workshop in Óbuda on Electrical and Power Engineering (CANDO-EPE), pp. 149–154.
https://doi.org/10.1109/CANDO-EPE47959.2019.9110967

Publisher's version: DOI: 10.1109/CANDO-EPE47959.2019.9110967

Off-field Testing of Grid Scenarios at Medium Voltage in Flexible AC Transmission Systems involving Wind Energy

Helge Lorenzen
⟺
Department of Engineering Sciences
Jade University of Applied Sciences
Wilhelmshaven, Germany
Lorenzen@Jade-Hs.de

Department of Electrical engineering, Information Technology and Cybernetics
University of South-Eastern Norway
Porsgrunn, Norway

Josef Timmerberg
Department Management, Information, Technology
Jade University of Applied Sciences
Wilhelmshaven, Germany
JT@jade-hs.de

Tim Lüken
Strategic Net Development
EWE NETZ GmbH
Oldenburg, Germany
Tim.Lueken@ewe-netz.de

Saba Mylvaganam
Department of Electrical engineering, Information Technology and Cybernetics
University of South-Eastern Norway
Porsgrunn, Norway
Saba.Mylvaganam@usn.no

***Abstract*—As a result of the geographical location of north-western Germany, the local grid operator EWE NETZ has a pioneer role with respect to the integration of renewable energy sources in existing AC transmission systems. About 7kWh out of 10kWh from EWE NETZ are from renewable sources, which are fed into existing AC transmission systems using FACTS (Flexible AC Transmission System). Currently, electricity from renewable sources such as on- and offshore wind energy farms, biomass, photovoltaics and hydropower are fed into existing power grids in northern Germany. This process drives the medium voltage grid networks into power utilization limits, leading to various operational problems of the modules used in the networks. In areas away from big cities, such as villages and small towns, the low load demand and the high value of power fed into the grid frequently leads to outages of medium power transformers and/or the associated switchgears. In addition, due to long transmission lines, the allowable limits of voltage escalations are often violated. In the context of FACTS, observations by EWE NETZ show that the number of curtailments within the last decade has increased by 7200%! There is an increasing need to study various unstable grid behaviours by looking at switching stations, switch gears, load impedances, frequency variations etc. with respect to varying levels of renewable energy fed into the grid. By emulating the scenarios encountered in the field using a dedicated laboratory at Jade University of Applied Sciences (JUAS), measurements, modelling and model predictive control can be performed successfully.**

***Index Terms*—Electric energy system, experimental technique, FACTS, renewable energy, feed power management, voltage control, symmetrical components, laboratory scale experiments.**

I. BACKGROUND

In conjunction with FACTS and behaviour studies of grids, the laboratory is designed for off-field testing of grid scenarios, to handle varying loads, voltage and frequency stability and reactive power management. Thus,

- control methods to circumvent unacceptable escalations of key parameters,
- different scenarios involving varying levels of renewable energy feeds,
- voltage variations (high and low) due to varying power consumptions (i.e. varying loads),
- feed management according to EISMAN and
- malfunctioning of sensors and actuators

can be tested in the laboratory without resorting to time consuming and expensive field tests.

II. EXPERIMENTAL DESIGN

To facilitate the testing of different scenarios, the area of the grid in the north-western part of Germany, - shown in Figure 1 - was studied in the NETZTEST Lab at JUAS shown in Figure 2 and Figure 3. The factors taken into account in this study, performed in the NETZTEST laboratory, are

- generated and consumed power,
- storage capacity in the region under scrutiny,
- short circuit voltages/powers,
- considerations of the ratios of resistive / reactive impedances and
- grid network structure.

The typical measurands in the NETZTEST lab are shown in Figure 4 and the measurement system used is shown in Figure 5

A. Design Goals

For testing the significant characteristics of the EWE grid network an emulation of it had to be achieved. For testing purposes a model region is selected as shown in Figure 1, to implement the algorithms, [1].

978-1-7281-4358-3/19/$31.00 ©2019 IEEE

B. Network Tuning

Based on data gathered for realizing these goals, a network topology has been conceived. Using one of the industry standard software for load flow computations (DIgSILENT PowerFactory) the grid network was studied closely looking for its performance under variations of selected parameters and identifying the particular combinations of these leading to critical situations. After identifying these "critical" sets of parameters, the scenarios were emulated by feeding these in a set of tuning operations in the NETZTEST lab.

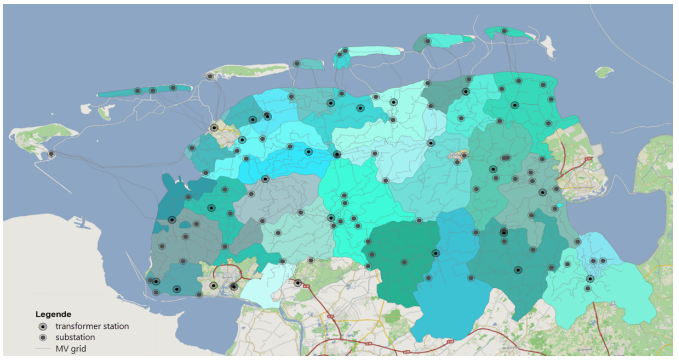

Fig. 1. The grid under scrutiny shown in the map of northern Germany for testing and modelling different scenarios.

Fig. 2. JUAS emulation laboratory for testing different scenarios

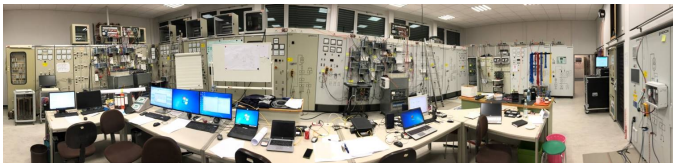

Fig. 3. The test laboratory in JUAS specifically upgraded for testing scenarios and control algorithms w.r.t FACTS in grids fed with renewable energy

C. Measurement Data Analysis

The variables (Vx, Ix, Px,Qx), with Vx representing voltage, Ix the current, Px and Qx the real and reactive power for all three phases, x= a, b and c were measured and analysed in this study. The values of Vx and Ix were sampled and measured with high resolution. For a selected time slot, all these parameters with their phase angles and amplitudes were studied. In external load studies all sequences were considered, i.e. zero, positive and negative sequences. For the current project, the focus was on the positive sequence. The symmetrical components have been calculated first according to the relevant test standard (IEC 61400-21-1 Annex C) then using the methods discussed in the next section leading to further analysis of the system.

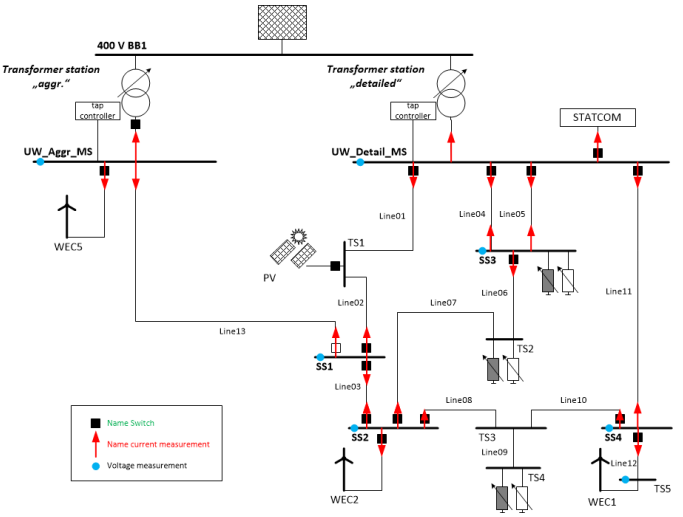

Fig. 4. Measurands for the system emulating FACTS scenario showing the essential parameters.

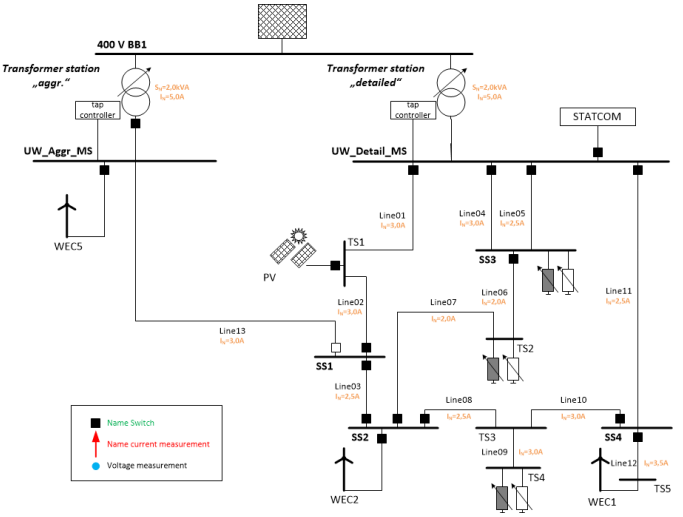

Fig. 5. Measurement system for tests of FACTS performance and control showing some of the nominal values.

III. Brief Background on Symmetrical Components

In the case of independent sinusoidal 3 phases, each phase (voltage or current) can be represented as a complex number with the amplitude $\hat{\Psi}$ and an angle ϕ.

$$\begin{aligned}\underline{\Psi} &= \hat{\Psi} \cdot e^{j\cdot(\phi_0+\omega t)} \\ &= \underbrace{\hat{\Psi} \cdot e^{j\cdot\phi_0}}_{\underline{\Psi}(t=0)} \cdot \underbrace{e^{j\cdot\omega t}}_{rotating\ component}\end{aligned} \tag{1}$$

which takes the following form using Euler's formula

$$\hat{\Psi} \cdot e^{j\cdot\phi_0} = x_c + j \cdot x_s \tag{2}$$

for the stationary part and for the rotating part (3) real and imaginary parts are defined by the t of the time axis and angular frequency ω.

$$e^{j\cdot\omega\cdot t} = cos(\omega \cdot t) + j \cdot sin(\omega \cdot t) \tag{3}$$

Substituting these values in equation (1) leads to

$$\begin{aligned}\hat{\Psi} \cdot e^{j\cdot\phi_0} \cdot e^{j\cdot\omega\cdot t} &= (x_c + j\cdot x_s)\cdot(cos(\omega\cdot t) + j\cdot sin(\omega\cdot t)) \\ &= x_c\cdot cos(\omega\cdot t) - x_s\cdot sin(\omega\cdot t) + j\cdot(...)\end{aligned} \tag{4}$$

For an unambiguous determination of x_c and x_s, it suffices to consider a solution for the real part of both sides of equation (4). So these values can then be used to estimate

$$\begin{aligned}\Psi &= real(\underline{\Psi}) \\ &= x_c\cdot cos(\omega\cdot t) - x_s\cdot sin(\omega\cdot t)\end{aligned}$$

$\Psi(t)$ is then found to be a linear combination of $sin(\omega t)$ and $cos(\omega t)$ (include the minus in x_s) as given below in (5).

$$\Psi = x_c\cdot cos\,(\omega t) + x_s\cdot sin\,(\omega t) \tag{5}$$

In the case of operational faults of switches, the system ends up in a process of stabilisation, whereby far away from the generator, the assumption $I_s'' = I_s$ is valid (the initial short-circuit ac is equal to the sustained short-circuit current).

Using the time constant τ for the stabilisation process, equation (5) can be expanded as given in equation (6).

$$\Psi = x_c\cdot cos(\omega t) + x_s\cdot sin(\omega t) + x_\tau\cdot e^{\frac{-t}{\tau}} \tag{6}$$

In the case of short intervals or very slow stabilisation, the argument in the exponential term vanishes due to a very small ratio $\frac{t}{\tau}$, and the exponential term becomes 1. Thus equation (7) takes the following form with a DC-component x_{DC} instead of an x_τ

$$\Psi = x_c\cdot cos(\omega t) + x_s\cdot sin(\omega t) + x_{DC}\cdot 1 \tag{7}$$

During the experiments with 3-phase systems, the last term x_{DC} is often useful, as it helps to account for the DC-components as well as for any offsets arising in different situations.

Assuming sample frequency f_s to be known and constant, with the fundamental frequency $f_0 \approx 50Hz$ and $\omega_0 = 2\pi f_0$. For each interpolated complex value a linear system of equations can be formed as given in equation (8) for phase "a" of a three phase physical quantity like voltage or current.

$$\underbrace{\begin{bmatrix} cos(\omega t_1), & sin(\omega t_1), & 1 \\ \vdots & \vdots & \vdots \\ cos(\omega t_n), & sin(\omega t_n), & 1 \end{bmatrix}}_{\mathbf{A}} \cdot \underbrace{\begin{bmatrix} x_{ca} \\ x_{sa} \\ x_{DCa} \end{bmatrix}}_{\mathbf{X}_a} \approx \underbrace{\begin{bmatrix} y_a(t_1) \\ \vdots \\ y_a(t_n) \end{bmatrix}}_{\mathbf{Y}_a} \tag{8}$$

$$\mathbf{A} = \begin{bmatrix} cos(\omega t_1), & sin(\omega t_1), & 1 \\ \vdots & \vdots & \vdots \\ cos(\omega t_n), & sin(\omega t_n), & 1 \end{bmatrix} \tag{9}$$

Equation (8) can be reformulated for X_a as given in equation (10) for phase a.

$$\mathbf{X}_a \approx \underbrace{\left(\mathbf{A}^T\mathbf{A}\right)^{-1}\cdot\mathbf{A}^T}_{\mathbf{B}}\cdot\mathbf{Y}_a = \mathbf{B}\cdot\mathbf{Y}_a \tag{10}$$

The matrices A and B are dependent on the sampling points of the sampling frequency f_s and the assumed fundamental frequency $\omega = 2\cdot\pi\cdot f_0$ and are related to each other as given in (11), with the superscript T indicating transpose operation.

The difference $t_j - t_{j-1} = \frac{1}{f_s}$ between the times of two consecutive rows of A results from the sampling frequency f_s. The estimate applies to the time $y_a(t=0)$. For online analysis in order to estimate always for the most recent sampling time, $t = t_n = 0$ is selected for the last row. For offline analysis it is obvious to estimate for the middle row and set $t_{\frac{n}{2}} = 0$.

$$\mathbf{B} = \left(\mathbf{A}^T\mathbf{A}\right)^{-1}\cdot\mathbf{A}^T \tag{11}$$

Equation (10) applies to the column vectors Y_b and Y_c containing samples from phase b and phase c as follows

$$\begin{aligned}\mathbf{X}_b &\approx \mathbf{B}\cdot\mathbf{Y}_b \\ \mathbf{X}_c &\approx \mathbf{B}\cdot\mathbf{Y}_c\end{aligned}$$

The evaluation of X for all 3 lines (a,b and c) of a transmission line system can be written [2] in the following compact form:

$$\begin{bmatrix} x_{ca} & x_{cb} & x_{cc} \\ x_{sa} & x_{sb} & x_{sc} \\ x_{DCa} & x_{DCb} & x_{DCc} \end{bmatrix} = \begin{bmatrix} b_{1,1} & \dots & b_{1,n} \\ b_{2,1} & \dots & b_{2,n} \\ b_{3,1} & \dots & b_{3,n} \end{bmatrix} \cdot \begin{bmatrix} y_{a1} & y_{b1} & y_{c1} \\ \vdots & \vdots & \vdots \\ y_{an} & y_{bn} & y_{cn} \end{bmatrix}$$

$$\begin{aligned}[\mathbf{X}_a, \mathbf{X}_b, \mathbf{X}_c] &= \mathbf{B}\cdot[\mathbf{Y}_a, \mathbf{Y}_b, \mathbf{Y}_c] \\ \mathbf{X} &= \mathbf{B}\cdot\mathbf{Y}\end{aligned} \tag{12}$$

A. Testing with synthetic data

Using the interval of time $-20ms < t < 20ms$ for a 50Hz signal, the matrix $\mathbf{X}$ given in equation (12) can be determined. The matrix $\mathbf{A}$ was precalculated under the erroneous assumption of the fundamental frequency being 40Hz. The values at $t = 0$ are directly taken from X. The other values are estimated by substituting X in equation (7). The deviation between the samples $y(t)$ and the estimates $\Psi(t)$ is clearly seen in Figure 6. The plot shown in Figure 8 shows a negligible deviation of angle at time $t = 0$.

By using the estimated value of X directly, instead of substituting in equation (7), the sampling window is shifted and the value of X is updated. With this method, the mean of frequency f_{est} from (13) is not the assumed frequency of 40Hz, but very close to the actual fundamental frequency (in our example 50Hz).

$$\begin{aligned}\Delta\phi &= \angle(\underline{\Psi}_{tk}, \underline{\Psi}_{t_{k-1}}) \\ \omega_{est} &= \Delta\phi\cdot f_s \\ f_{est} &= \frac{\omega_{Est}}{2\pi}\end{aligned} \tag{13}$$

A new estimate of the complex values using matrices A and B based on the improved frequency provides the findings according to Figure 9. An influence of the constant summand x_{DC} of equation (7) is not recognizable, since this coefficient always remains negligibly small with time-invariant signals without a DC component.

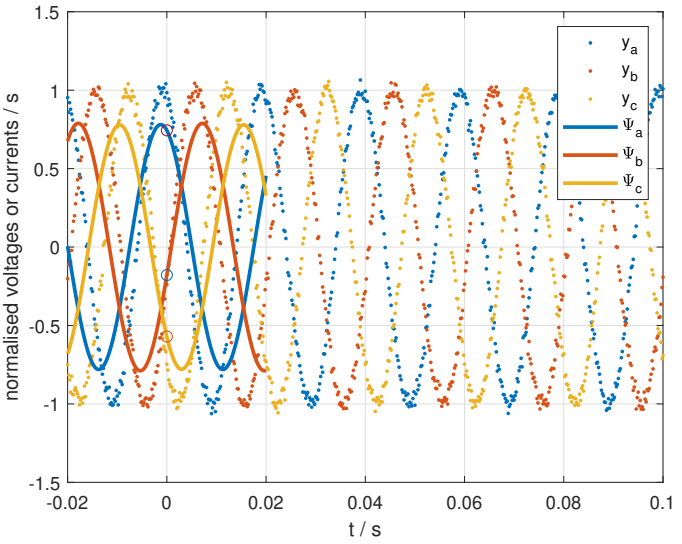

Fig. 6. Using synthetic signals showing samples v and fit $\Psi(t=0)$ using the phasor equation (1)

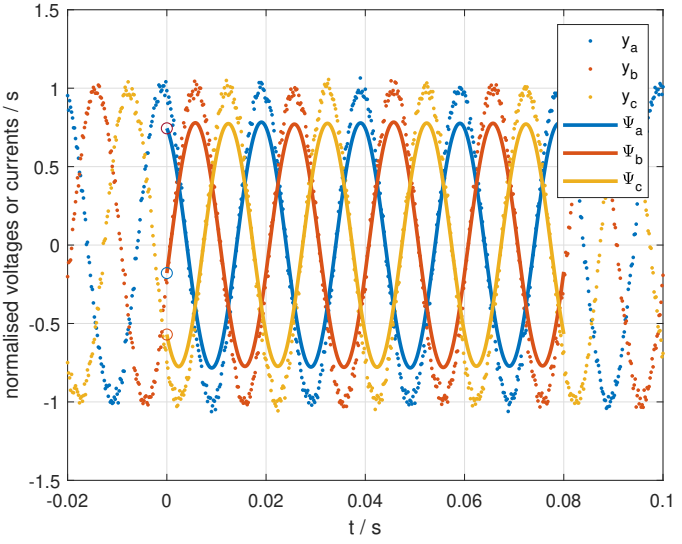

Fig. 7. Using synthetic signals showing samples vs fit. Compute $\Psi(t)$ for each t in the interval [20ms,80ms] applying (12) to samples in [t-20ms, t+20ms]

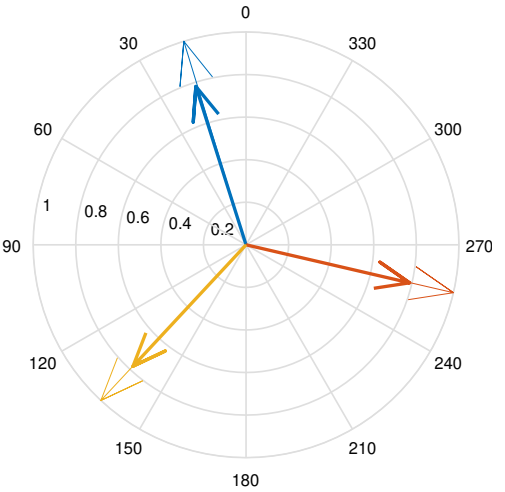

Fig. 8. Phasor for the components $\underline{\Psi}(t=0)$ shown in Figure 6 and Figure 7 (see bullets and graphs with corresponding color at $t=0$).

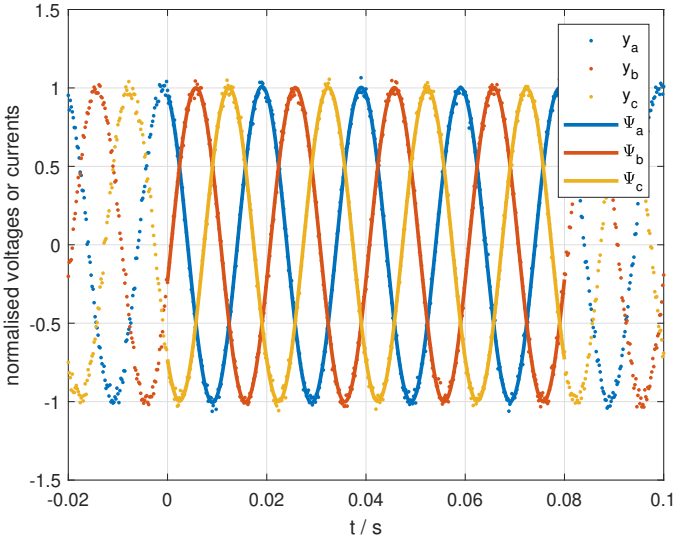

Fig. 9. Samples used identical to those used in Figure 7. Instead of the assumed frequency of 40Hz, improved estimates using (13)

B. Tests with signals sampled in the laboratory during asymmetric faults in the experimental grid.

For the following time series typical grid fault sequences were created. Each fault sequence begins with a single-phase to ground fault with residual voltage at the measuring location. This happens in about a second. Every second single phase ground fault transits into a phase to phase short with earth contact, also pending for a second. For the analysis of this demonstration, the measurement data are converted into complex time series by means of the method just described. This provides the complex interpolations for $\underline{\Psi}_v(t)$ and $\underline{\Psi}_i(t)$. Accordingly, the amount of $\underline{\Psi}(t)$ delivers (14) directly the fit for amplitudes as shown in Figure 11

$$\hat{v}(t) \approx |\underline{\Psi}_v(t)|$$
$$\hat{i}(t) \approx |\underline{\Psi}_i(t)| \tag{14}$$

The product of the complex values of V and I gives the complex powers for each conductor of the three phase system.

$$\underline{S} = \underline{V} \cdot \underline{I}^* \tag{15}$$
$$= \frac{\hat{\underline{V}}}{\sqrt{2}} \cdot \frac{\hat{\underline{I}}^*}{\sqrt{2}} \tag{16}$$
$$= \frac{1}{2} \cdot \hat{\underline{V}} \cdot \hat{\underline{I}}^* \tag{17}$$

In case of asymmetry in the transmission line system, the symmetrical components are used instead of line values. The symmetrical components are estimated using the line values

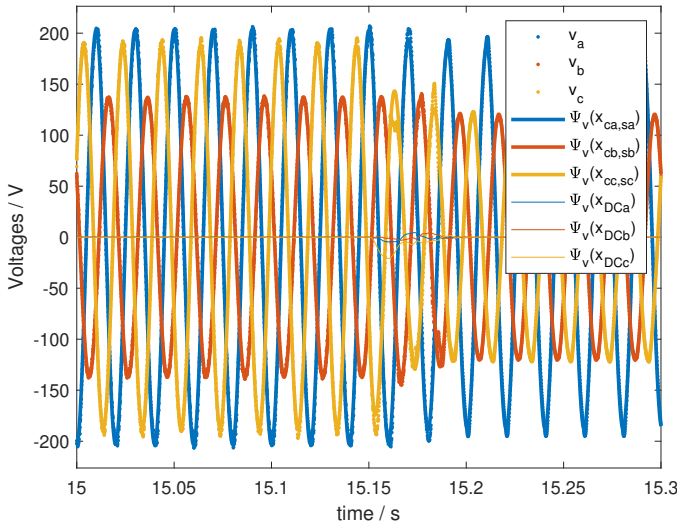

Fig. 10. Measurement data and interpolated values of the line voltages; transition from "line to ground" to "phase to phase to ground". Clear indication of the DC-component in stationary situation.

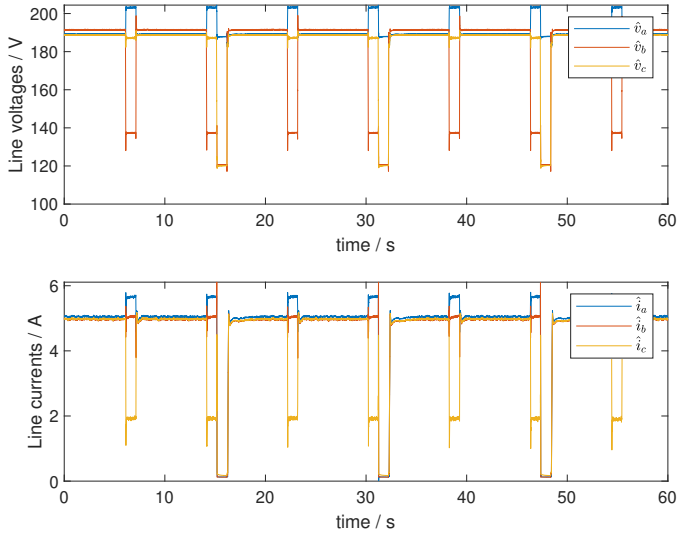

Fig. 11. Conductor current and external conductor voltage in the case of asymmetrical errors measured directly on a wind energy plant.

and are represented by using the inverse of the Fortescue matrix (NB. order of the indices 0,1,2).

$$\begin{bmatrix} \underline{\Psi}_1 \\ \underline{\Psi}_2 \\ \underline{\Psi}_0 \end{bmatrix} = \mathbf{F}^{-1} \cdot \begin{bmatrix} \underline{\Psi}_a \\ \underline{\Psi}_b \\ \underline{\Psi}_c \end{bmatrix} \tag{18}$$

where

$$\mathbf{F}^{-1} = \frac{1}{3} \cdot \begin{bmatrix} 1 & 1 & 1 \\ 1 & a & a^2 \\ 1 & a^2 & a \end{bmatrix}$$

and

$$a = e^{\frac{j \cdot 2 \cdot \pi}{3}}$$

The values of the symmetrical components of the voltage and current typical of the faults under study are shown in Figure 12

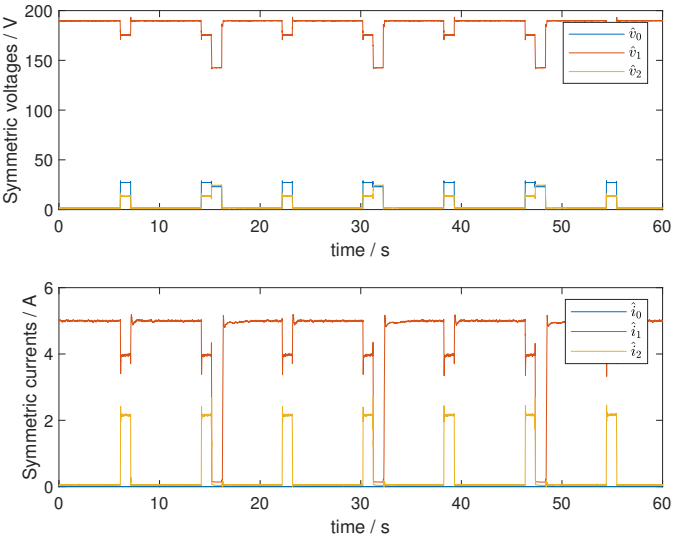

Fig. 12. Amplitudes of all three symmetrical components of the voltages and currents in the case of asymmetrical faults.

Using the values of voltages and currents , using (17), the values of the active and reactive power can be calculated.

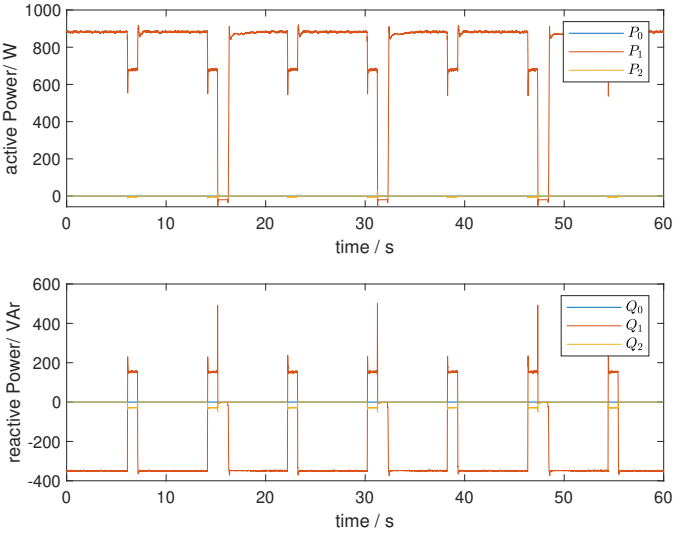

Fig. 13. Active and reactive powers displayed in symmetrical components corresponding with currents and voltages in Figure 12

IV. SOME RESULTS

A. Analysis of the FACTS response of a wind turbine when an unbalanced error occurs.

Figure 10 shows the instantaneous values of the voltages at a FACTS-capable wind turbine as well as corresponding interpolations Ψ_v. As can be seen more clearly in Figure 11, the amplitude of voltage $\hat{v}_b$ is significantly reduced at time $t = 15s$. The reason for this is a remote ground fault.

As can be seen in the lower half of Figure 11, the wind turbine continues to feed into the grid despite the fault. This is called "Fault Ride Through", [3]. The plant does a lot more. With fault entry, the current is unbalanced. It is noticeable that only the current in the healthy electrical conductors change.

The usefulness of this behaviour becomes apparent when looking at the symmetrical components. As can be seen in Figure 12, the positive sequence voltage is reduced by the fault; the asymmetry is known to be recognizable as negative sequence voltage. Also, a zero system component occurs with fault onset in the onset of fault in the line voltage.

As can be seen in Figure 13, the current leads to a significant feed-in of reactive power into the positive sequence, thus supporting the voltage. For the negative sequence this behaviour results in a negative reactive power, which has a reducing effect on the negative sequence voltage, i.e. the asymmetry. Due to the permissible limits for the current, a reduction of the injected active power must be accepted for the supply of reactive power. The active power not transmitted must be dissipated by a chopper.

At time $t = 15.2s$, the single-pole fault changes into a two-pole fault. The wind turbine is parameterized in accordance with the specifications of the grid operator so that the inverter current is suddenly blanked out in the case of this type of fault. Thus, the wind turbine also behaves in principle but gets into a critical condition. The entire generator power must be dissipated by the chopper, which would lead to an emergency shutdown of the wind turbine after a few seconds due to the pertainign enormous heat. The zero system does not appear neither at the current nor at the active power or reactive power. Of course, this has to be the case because this type of wind turbine feeds in via a transformer with the YD5 vector group.

B. Assessment of grid control

With currents held at nominal values with escalations up to 1.15 of nominal value for short periods and voltages within 0.95 to 1.05 p.u, some experiments were conducted. With these values, some of the tests yielded the results shown in Figure 14 to Figure 17, showing the transformer and line overloads, voltage stability and reactive power management. As an example, overloading the transformer by more than 5% is shown by the gray curve marked with an arrow in Figure 14. The significant reduction achieved by controller intervention is recognizable as well.

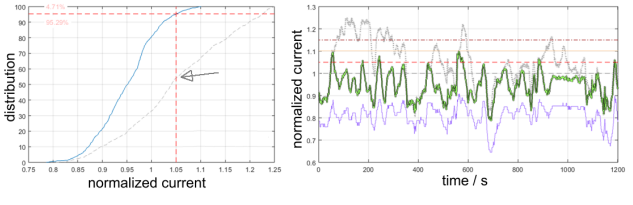

Fig. 14. Distribution (left) and time series(right) testing FACTS Scenario with transformer overload in NETZTEST lab at JUAS

Figure 15 shows the corresponding success of the controller in reducing line overloads. The values of the grey line here correspond to the maximum overload when considering all lines.

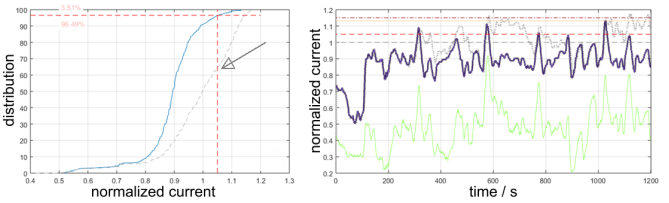

Fig. 15. Distribution (left) and time series(right) testing FACTS Scenario with line overload in NETZTEST lab at JUAS

Figure 16 shows the reduction of the voltage band violation by active power reduction in the generators, achieved by the intervention of one of the tested grid controllers. Here at one-second averages, a reduction from 68% down to 5.5% and for one-minute averages even a reduction from 56% to zero was achieved. As actuator, a windturbine with a static compensator (STATCOM) system is available at the bus-bar of the substation, for providing reactive power in cases of voltage variations. The set-point for the STATCOM is determined by a characteristic curve of reactive power parameterized in the controller as a function of the active power transmitted.

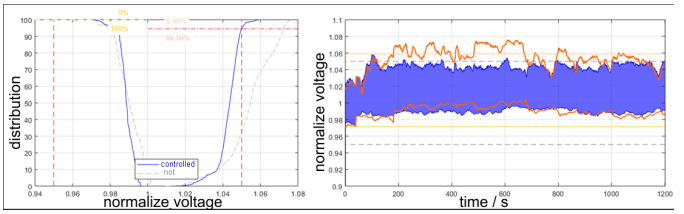

Fig. 16. Voltage stability tests in NETZTEST lab at JUAS

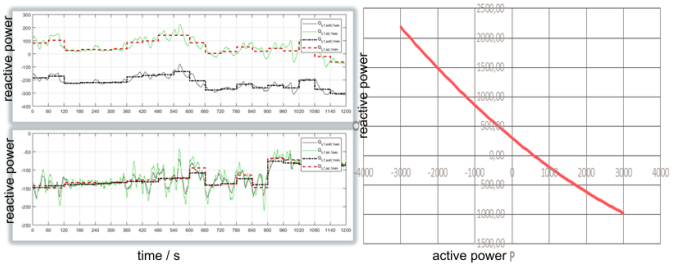

Fig. 17. Reactive power management tests in NETZTEST lab at JUAS, setpoint and actual values over different times averaged

REFERENCES

[1] Tim Lüken. "Smart controls for distribution systems with high share of RES",DFBEW conference Paris, 24th of November 2016

[2] Gilbert Strang. 18.06 Linear Algebra. Spring 2010. Massachusetts Institute of Technology: MIT OpenCourseWare, https://ocw.mit.edu. License: Creative Commons BY-NC-SA.

[3] D. McMullin and K.Pierros,"Voltage control with wind power plants - current practice wie type IV wtgs in UK an Ireland", Workshop on Large-Scale Integration of Wind Power into Power Systems as well as Transmission Networks for Offshore Wind Power Plants, London, UK, Oct. 2013